Atmos. Chem. Phys. Discuss., https://doi.org/10.5194/acp-2019-3
Manuscript under review for journal Atmos. Chem. Phys.
Discussion started: 7 January 2019

Atmospheric Chemistry and Physics Discussions

Temperature Effects on Sulfuric Acid Aerosol Nucleation and Growth: Initial Results from the TANGENT Study

Lee Tiszenkel[1], Chris Stangl[2], Justin Krasnomowitz[2], Qi Ouyang[1], Huan Yu[3], Michael J. Apsokardu[2], Murray V. Johnston[2], Shan-Hu Lee[1,4,*]

[1]Department of Atmospheric Science, University of Alabama in Huntsville, Huntsville, AL
[2]Department of Chemistry and Biochemistry, University of Delaware, Newark, DE
[3]School of Environmental Science and Engineering, Nanjing University of Information Science and Technology, Nanjing, China
[4]Department of Environmental Science and Engineering, Fudan University, Shanghai, China

Correspondence to: Shan-Hu Lee (shanhu.lee@uah.edu)

Abstract. New particle formation (NPF) consists of two steps: nucleation and subsequent growth. At present, chemical and physical mechanisms that govern these two processes are not well understood. Here, we report initial results obtained from the TANGENT (Tandem Aerosol Nucleation and Growth Environment Tube) experiments. The TANGENT apparatus enables us to study these two processes independently. The present study focuses on the effects of temperature on sulfuric acid nucleation and further growth. Our results show that lower temperatures enhance both the nucleation and growth rate. However, under temperatures below 268 K the effects of temperature on the nucleation rate become less significant and the nucleation rate becomes less dependent on RH, indicating that particle formation takes place via barrierless nucleation at lower temperatures. We also examined the growth of newly formed particles under differing temperature conditions for nucleation and further growth. Our results show that newly nucleated clusters formed at low temperatures can indeed survive evaporation and grow in a warmer environment in the presence of SO_2 and ozone, strongly implying that some heterogeneous reactions involving nanoparticles affect growth of newly formed particles.

1. Introduction

Atmospheric nanoparticles affect human health and air quality. Newly formed particles can contribute to approximately 30-70% of cloud condensation nuclei (CCN) in the atmosphere (Gordon et al., 2017; Merikanto et al., 2009; Wang & Penner, 2009; Yu & Luo, 2009). NPF takes place via two steps: initial nucleation (formation of critical clusters) and subsequent growth of nucleated clusters (Kulmala et al., 2013). At present, chemical and physical mechanisms that govern these two processes, as well as the identity of chemical precursors involved in these processes, are still not well understood (Yu et al., 2017b; Zhang et al., 2012). Current global models fail to represent NPF in the atmosphere for a wide range of temperature and RH conditions and for different emissions of biogenic and anthropogenic precursors due to a lack of observations. For example, models predict frequent NPF during the summer in mixed deciduous forests in the United States (Yu et al., 2015), while field

observations show an absence of NPF in this region (Kanawade et al., 2011; Lee et al., 2016). Also, current NPF theories are unable to explain the frequent NPF observed in extremely polluted megacities (Kulmala et al., 2017; Yu et al., 2017b).

Temperature and RH are the key thermodynamic properties of aerosol formation and growth (Seinfeld & Pandis, 2016). Nucleation rate (J) is a function of temperature and the Gibbs free energy barrier of cluster formation. At lower temperatures, Gibbs free energy barriers become lower and critical cluster diameters become smaller. Condensational species can affect aerosol growth differently at different temperatures because their saturation vapor pressures are dependent on temperature. For water, RH is the same as saturation ratio and chemical activity. Laboratory experiments of aerosol nucleation and growth as a function of temperature and RH remain limited, although these observations are critically needed in global models to correctly parameterize NPF under various altitude, latitude and seasonal conditions. Aerosol nucleation experiments are extremely challenging due to various experimental difficulties, including contamination of base compounds (Erupe et al., 2011; Yu et al., 2012). At present there is a lack of consistency between different experiments from different groups and even from the same groups using the same experimental setup. The lack of reproducibility and consistency of the nucleation experiments greatly hinders our understanding of nucleation mechanisms.

Duplissy et al., (2016) conducted studies of binary homogeneous nucleation of sulfuric acid and water, with and without ions in the CLOUD (Cosmics Leaving OUtdoor Droplets) chamber at different temperatures ranging from 207 to 299 K and RH between 11% - 58%. At lower temperatures both ion nucleation and neutral binary nucleation are at the kinetic regime, while at higher temperatures J is strongly dependent on $[H_2SO_4]$, indicating there are high Gibbs free-energy barriers at these temperatures. At the nucleation regime, nucleation rates are strongly dependent on RH. Kürten et al., (2016) reported the temperature dependence of ternary nucleation in the CLOUD chamber, at the temperature from 208 to 298 K, $[H_2SO_4]$ between 10^5 and 10^9 cm^{-3}, and $[NH_3]$ up to ~1400 pptv. At 208 K, J reached the threshold of 1 cm^{-3} s^{-1} at a $[H_2SO_4]$ of ~3×10^6 cm^{-3} for the binary case, and at $[H_2SO_4]$ of ~5×10^5 cm^{-3} for the ternary case with $[NH_3]$ of 5 pptv. At 298 K, RH has strong effects on the measured J for both charged and neutral ternary nucleation, because the increase in RH could lead to a displacement of NH_3 from the stainless-steel walls in the CLOUD chamber and lead to an elevated NH_3 background level and consequently to higher J.

Laboratory experiments of growth rates (GR) of newly nucleated particles are very sparse. (Skrabalova et al., 2014) studied GR of newly formed particles in a flow tube at the temperature between 283 to 303 K and RH of 1% and 30%, designated as "dry" and "wet" conditions, respectively. $[H_2SO_4]$ was varied between 2×10^8 cm^{-3} and 1.4×10^{10} cm^{-3}. They found different effects of RH on GR; at $[H_2SO_4]$ below 10^9 cm^{-3}, growth is promoted in drier conditions, whereas at $[H_2SO_4]$ higher than 10^9 cm^{-3}, growth favours wetter conditions. Yu et al., (2017a) performed flow tube experiments of sulfuric acid aerosol nucleation, at the temperature from 248 to 313 K and RH from 1% to 79%, under minimal base concentrations ($[NH_3]$ < 23 pptv, methylamine < 1.5 pptv, and dimethylamine < 0.52 pptv). This study provides for the first time the temperature and RH dependence of both J and GR. J shows the following dependence within the experimental conditions:

$$J = 10^{41.8}[\mathrm{RA}]^3[\mathrm{RH}]e^{\frac{-2.4\times10^4}{T}}, \quad (1)$$

where RA is relative acidity (or saturation ratio) of sulfuric acid, and T temperature. Their results show that *GR* is independent of temperature below 290 K, but significantly decreases at temperatures above 290 K. RH has a moderate effect on *GR*.

Another important perspective of temperature effects on NPF is the effects of temperature on evaporation of newly nucleated clusters and nanoparticles. The lack of local NPF events in Amazon forests has been a confounding observation for many years (Rizzo et al., 2018) and yet there are reservoirs of nuclei mode particles at the surface which do not form typical "banana" plots of aerosol size distributions observed elsewhere (Martin et al., 2016). Understanding the origin of these nuclei mode particles has been a subject of recent studies. (Wang et al., 2016) reported that while NPF does not take place in Amazon forests at the surface level during the dry and wet season, NPF takes place in the colder free troposphere; these newly formed particles can be transported down to the boundary layer to become a reservoir of nanoparticles at the surface. A subsequent question is whether newly nucleated clusters and nanoparticles in the free troposphere can survive evaporation during their transport to the warmer boundary region. At present, the temperature effects on the growth of newly formed particles crossing different temperature regions have not been examined in a controlled laboratory environment.

Here, we present the initial results of the TANGENT experiments conducted during the Intensive Observation Period (IOP) study in June and July 2018. In the present study, we report the temperature effects on *J* and *GR* of sub-2 nm particles in the nucleation tube. We also discuss how temperature differences in the nucleation and growth tube affect the potential evaporation of newly nucleated clusters while these clusters are transported from the colder to the warmer temperature region.

2. Methods

2.1 The TANGENT Experimental Setup

Figure 1 shows the schematic diagram of the TANGENT apparatus. The TANGENT consists of the two flow tubes (FT) to enable studies of nucleation (FT-1) and subsequent growth (FT-2). The nucleation tube was built by the University of Alabama in Huntsville, and the growth tube by University of Delaware.

The experimental setup of the nucleation region (FT-1) was based on (Benson et al., 2009; Benson et al., 2008; Benson et al., 2011; Erupe et al., 2011; Young et al., 2008; Yu et al., 2017a; Yu et al., 2012). It consists a photolysis region where H_2SO_4 is generated photochemically and monitored followed by a temperature-controlled nucleation tube. In the photolysis region, OH radicals were produced via photodissociation of water vapor in a quartz tube using a mercury lamp (Pen-Ray Model 11SC-1). The mercury lamp was located in a temperature-controlled enclosure filled with a constant nitrogen flow. UV intensity was adjusted with an aperture over the slit in the enclosure exposing the quartz tube to the UV lamp. UV intensity was monitored with a CsI phototube (Hamamatsu Model R5764) and picoammeter (Keithley 6732). Measurements of UV intensity were taken to ensure consistency between experimental trials. SO_2, O_2 and N_2 gases were introduced to the flow tube immediately after the photolysis region. H_2SO_4 forms from the SO_2 + OH reaction. Heating tape was applied to the H_2SO_4 production region to suppress nucleation prior to entering the temperature-controlled nucleation zone. The H_2SO_4 production region was monitored

with a condensation particle counter (CPC, TSI 3776) and particle sizing magnifier (PSM, Airmodus A09) to ensure no particles were formed before the flow entered the nucleation region.

H_2SO_4 concentrations at the beginning of the nucleation tube were measured with a nitrate-based chemical ionization mass spectrometer (CIMS) based on (Eisele and Tanner, 1993) continuously during the experiments. Calibration of [H_2SO_4] with the nitrate-CIMS was described previously by (Young et al., 2008). The CIMS was operated with an inlet flow of 5.0 SLPM and an ion-molecule reaction time of 0.05 s. The lower limit of detection was calculated to be ~1x10^5 cm^{-3}. The overall uncertainty of the H_2SO_4 measurements was estimated at ±60%.

No base compounds were added, but base compounds were present in the flow tube as impurities likely generated from deionized water used for H_2SO_4 production and RH control (Erupe et al., 2011; Yu et al., 2012). NH_3 and amines were not measured during the 2018 IOP, but they were measured under very similar experimental conditions during the entire 2017 IOP with an ethanol-CIMS at the beginning of the nucleation tube (You et al., 2014; Yu & Lee, 2012). Detection limits of NH_3/amines in our CIMS were pptv or sub-pptv with a 1-min integration, as previously discussed elsewhere (Benson et al., 2010; Erupe et al., 2011; You et al., 2014; Yu & Lee, 2012).

The nucleation tube is an 80 cm long Pyrex glass tube with an i.d. of 4.85 cm. The temperature of the nucleation tube was controlled with a circulating bath and a water-based potassium formate heat transfer fluid (Dynalene HC-50, Dynalene, Inc.) to adjust the temperature between 258 and 297 K. RH was adjusted by directing some of the dry nitrogen makeup flow through deionized water in a water bubbler. Thus, in our experimental setup, changes in RH in the nucleation tube did not affect the OH radical concentrations in the photolysis region. Temperature and RH probes (CS-215, Campbell Scientific) were used to monitor the conditions at the beginning of the photolysis region, as well as at the end of the nucleation region. An additional temperature and RH probe (Traceable, Fisher Scientific) was applied inside the nucleation tube to confirm the RH. Residence time in the nucleation region (FT-1) was 45 s.

Particle concentrations at the exit of FT-1 were measured with a PSM [Vanhanen et al., 2011]. The PSM saturator flow was operated with a 240-step cycle between 0.1 - 0.9 SLPM at a rate of 1 s per step, giving saturator flow dependent cut-off sizes between 1.26 nm and 2.85 nm. These cut-offs were resolved to six size bins in an inversion method based on *Lehtipalo et al.*, [2014], producing size distributions with six size bins: 1.26 - 1.53 nm, 1.53 - 1.79 nm, 1.79 - 2.06 nm, 2.06 - 2.32 nm, 2.32 - 2.59 nm, and 2.59 - 2.85 nm. Particle concentrations were also monitored with a scanning mobility particle sizer (SMPS) consisting of a differential mobility analyser (DMA, TSI 3080) and a CPC (TSI 3776). However, under the typical experimental conditions, particles above 3 nm in diameter did not appear even with the most favourable conditions for nucleation and growth (e.g., high [H_2SO_4], high RH and low temperature).

During the experiments, [H_2SO_4] was varied by adjusting the aperture on the mercury lamp housing (hence varying [OH]) at a fixed [SO_2], allowing for a range of [H_2SO_4] spanning roughly one order of magnitude for a given dilution of SO_2. [H_2SO_4] was further varied by adjusting the SO_2 dilution, allowing for measurements spanning [H_2SO_4] of 10^6 to 10^9 cm^{-3}. The PSM measurements showed that each experimental condition was "stabilized" typically after ~30 min for a specific set of [H_2SO_4], RH and temperature.

Atmos. Chem. Phys. Discuss., https://doi.org/10.5194/acp-2019-3
Manuscript under review for journal Atmos. Chem. Phys.
Discussion started: 7 January 2019

The photolysis and nucleation tubes were cleaned thoroughly with deionized water, citric acid solution and ethanol and allowed to dry for 24 hours while heated to 60 °C with pure N_2 flowing through the flow tube. Between experiments, the photolysis and nucleation tubes were continuously flushed with dry vaporized liquid nitrogen. A constant flow of N_2 was passed through the experimental apparatus at all times during the IOP to ensure that the conditions inside the tube would remain constant and there would be no intrusion of room air.

The nucleated clusters (smaller than 2 nm) were transported to the growth tube (FT-2) for further growth with an extended residence time (4 min). FT-1 and FT-2 were coupled with an 8-inch stainless steel tube with additional inlet ports for injection of ozone, zero air and SO_2. The growth tube was described by (Krasnomowitz et al., 2018) . The growth tube consists of a 1.52 m long and 0.2 m i.d. fused quartz tube fitted with stainless steel funnels on each end that reduce the i.d. down to 0.051 m. The total volume of the tube and entrance and exit funnels is 52.4 L, giving a surface-to-volume ratio of 0.24 cm^{-1}. The 8-inch straight tube fitting allows carrier/reactant gases to enter the tube via an axial inlet port and continuous flow through the entire length of the reactor during the course of an experiment. The end of the tube was attached to an ozone monitor (Thermo Scientific 49i), a hygrometer (Traceable, Fisher Scientific), and an SMPS (TSI 3938, 3788).

2.2 Calculations of Nucleation (J) and Growth Rate (GR)

Calculations of *J* were made based on *Yu et al.*, [2017]. Briefly, *J* was calculated according to the following approximation:

$$J_0 \approx N_{tot} \times nk_L, \quad (2)$$

where J_0 represents the nucleation rate corresponding to the initial sulfuric acid concentration ($[H_2SO_4]_0$) measured at the beginning of the nucleation tube, N_{tot} the total number concentration of particles detected at the end of the nucleation region, n the nucleation theorem power determined by the linear fit between Log N_{tot} and Log $[H_2SO_4]_0$, and k_L the diffusion-limited, pseudo first-order wall loss coefficient (Hanson and Eisele, 2000). Our k_L was typically 0.01 s^{-1}.

To calculate GR, the critical cluster size was determined experimentally, with the critical cluster size corresponding to the y-intercept of the linear fit between the mean particle diameter, D_p, and the $[H_2SO_4]_0$ (e.g., Fig. 3). D_p was obtained using the inversion of the PSM size distribution measured at the end of FT-1. GR was calculated by the difference between the critical size and D_p divided by the nucleation time.

The growth rate factor k_G, defined as the ratio of GR/$[H_2SO_4]$, was determined by the expression derived by (Yu et al., 2017):

$$k_G = \frac{\Delta D_{p,tr} \times 10^7 cm^{-3}}{[H_2SO_4]_0} \frac{k_L}{1-e^{-nk_L t_r}}, \quad (3)$$

$\frac{\Delta D_{p,tr}}{[H_2SO_4]_0}$ was experimentally determined by plotting D_p against $[H_2SO_4]_0$ (e.g., Fig. 3), which gives a linear relationship. Thus, the k_G is the product of the slope and $\frac{k_L \times 10^7\ cm^{-3}}{1-e^{-nk_L t_r}}$.

Atmos. Chem. Phys. Discuss., https://doi.org/10.5194/acp-2019-3
Manuscript under review for journal Atmos. Chem. Phys.
Discussion started: 7 January 2019

3. Results and Discussion

Table 1 shows the typical experimental conditions used in the FT-1 (nucleation tube) and FT-2 (growth tube) during the 2018 IOP study. In the nucleation tube, temperature was varied from 258 to 297 K and RH from 4% to 85%. [H_2SO_4] spanned from 10^6 to 10^8 cm^{-3}, corresponding to RA of 10^{-5} to 10^{-2}. RA was calculated using the sulfuric acid saturation vapor pressures provided by (Vehkamaki et al., 2002). The CIMS-measured NH_3 (during the 2017 IOP) was 14.2 ± 6.7 ppt (Fig. 2). Thus, the ratio of [NH_3]/[H_2SO_4] ranged from 0.6 to 268. According to (Schobesberger et al., 2015) and (Dunne et al., 2016), these ratios represent ternary nucleation and some nucleation in a transition regime between binary and ternary, when considering only the effects of NH_3 (without amines). Overall, the measured nucleation rates ranged from 10 - 10^5 cm^{-3} at higher temperatures and lower [H_2SO_4] up to 10^5 cm^{-3} at lower temperatures and higher [H_2SO_4]. The observed GR ranged from 1 to 80 nm h^{-1}. The growth tube (FT-2) was kept at room temperature (297 K) and dry conditions (RH of 10%). SO_2 was added in the range from 100 ppbv to 5 ppmv and ozone from 0 to 248 ppbv.

Figure 3 shows the measured D_p with the PSM at the end of FT-1 as a function of the initial $[H_2SO_4]_0$ at the temperature between 258 and 297 K. $[H_2SO_4]_0$ was varied from 8 x 10^6 cm^{-3} to 7 x 10^7 cm^{-3}. The RH was kept in relatively narrow range between 20% and 30%. The y-intercept in Fig. 3 indicates a critical cluster diameter of 1.67-1.68 nm. This critical size is consistent with Kulmala et al. (2013) and Almeida et al. (2013), which determined critical cluster diameters of 1.5 $\pm$ 3 nm and 1.7 nm, respectively. Larger mean diameters were detected under lower temperatures for a given $[H_2SO_4]_0$. Previously, (Glasoe et al., 2015; Yu et al., 2017a) have also shown increasing GR with increasing [H_2SO_4] from flow tube experiments. The slope of D_p vs. $[H_2SO_4]_0$ increased with each 10 degree decrease in temperature over the course of these experiments. Thus, the growth rate factor k_G also increased with subsequent temperature decreases (e.g., from 1.27 at 297 K to 12.6 at 258 K). These results indicate that lower temperatures promote the faster growth of particles due to the reduction in saturation vapor pressures of H_2SO_4 at lower temperatures.

Figure 4 shows the relationship of Log *J* vs. Log RA for different temperatures. Experiments were conducted at 10 K intervals, starting from 297 K down to 258 K for RH between 41% and 45%. Across all temperature and RH experiments conducted, in general, *J* values were shifted 2 to 3 orders of magnitude above previous literature values [Yu 2017, Brus 2011]. Based on our measured NH_3 and amine concentrations (Fig. 2), this upward shift is consistent with the nucleation rate enhancement due to NH_3 concentrations on the order of 20 to 30 pptv, dimethylamine concentrations on the order of 1 to 2 ppt reported by other studies (Glasoe et al., 2015). There was a consistent relationship between Log *J* and Log RA. Except for 288 K and 297 K, where the slope of Log *J* vs. Log RA was approximately 2, slope was 3 for all trials, with the best-fit lines shifting towards higher values of RA as temperature decreased. Hanson and colleagues provided comprehensive analysis of Log *J* vs. Log RA (or Log [H_2SO_4]) obtained from flow tube studies (Glasoe et al., 2015; Zollner et al., 2012). In general, flow tube studies from various groups have shown slopes between 3-6 for the ternary system (Berndt et al., 2014; Brus et al., 2010; Erupe et al., 2011; Glasoe et al., 2015; Hanson et al., 2017; Yu et al., 2012; Zollner et al., 2012). Using the CLOUD experiments, (Almeida et al., 2013; Dunne et al., 2016; Kirkby et al., 2011) also showed the slope of 3 for the ternary system. This slope is consistent with

the base-stabilization mechanism provided by (Chen et al., 2012; Jen et al., 2014; Jen et al., 2016) that the bottleneck clusters contain 3-4 H_2SO_4 molecules with at least one base molecule. It was previously believed that the slope of Log *J* vs. Log RA dictates the amount of H_2SO_4 molecules present in the critical cluster based on classical nucleation theory (CNT) (Kashchiev, 1982; McGraw & Zhang, 2008), which then would imply here that the critical cluster contains three H_2SO_4 molecules for the ternary system. However, more recent work by (Malila et al, 2013, Vehkamaki et al, 2012) has shown that this conclusion may be an oversimplification of the mechanism of particle formation resulting from an application of CNT with an incomplete understanding of the free energy maxima and minima. As a result, there is caveat when the critical cluster composition is determined by the simple relationship between *J* and $[H_2SO_4]$.

Figure 5 shows the measured *J* as a function of temperature for $[H_2SO_4]$ between $2x10^7$ and $3x10^7$ cm^{-3} and RH between 15% to 45%. *J* increased with the decreasing temperature in the temperature range above 268 K. The higher *J* at lower temperatures is consistent with predictions from CNT (Seinfeld & Pandis, 2016). However, a shift in slope is visible around 268 K, indicating that the dependence of *J* on temperature becomes less significant at low temperatures. The variation seen across RH at higher temperatures also becomes negligible below this temperature. Thus, these results indicate that at temperatures below 268 K, Gibbs free energy barriers are reduced significantly. This is consistent with (Duplissy et al., 2016) that found barrierless particle formation at lower temperatures. As discussed above, the base contamination present in the conditions for this study resulted in elevated *J* values, which also resulted in this barrierless kinetic nucleation occurring at a relatively higher temperature.

In order to determine whether newly formed particles nucleated at lower temperatures can survive downward transport to warmer temperature conditions, we conducted experiments using two different temperatures in FT-1 (268 K) and FT-2 (297 K) (Fig. 6). The average particle concentration coming out of FT-1 was $2x10^5$ cm^{-3} with a median diameter of 1.90 nm at $[H_2SO_4]_0$ of $6x10^7$ cm^{-3} and RH of 10%. These newly formed particles were further mixed with an additional zero air flow at a 1:6 dilution. The $[SO_2]$ was 83 ppbv and the ozone level was varied from 0 to 248 ppbv in FT-2. No particles were observed coming out of FT-2 when ozone was absent, indicating that SO_2 alone does not cause nucleation and growth of clusters. However, in the presence of ozone and SO_2, continuous nucleation and further growth of transported clusters took place in FT-2. The particle concentration measured at the end of FT-2 was closely correlated with the ozone concentration: the particle concentration ranged from $3x10^2$ cm^{-3} (with D_p of 2.8 nm) at the lowest ozone of 28 ppbv up to $5x10^4$ cm^{-3} (D_p of 3.4 nm) at the maximum ozone of 248 ppbv. Thus, the particle concentration in FT-2 at the highest ozone was even greater than that coming out of FT-1 after dilution, indicating that a high ozone load resulted in additional nucleation and the further growth of clusters in FT-2. This could be the result of the remaining H_2SO_4 vapour passing through to FT-2, but we excluded this possibility. After considering wall loss in FT-1 and the 1:6 dilution FT-2, $[H_2SO_4]$ in FT-2 was estimated to be $1.15x10^6$ cm^{-3}, which can result in *J* only on the order of 10^1 cm^{-3} s^{-1} at room temperature and the dry condition, as shown from the results obtained in FT-1 (e.g., Fig. 4). However, the measured formation rate (*J*) of particles in FT-2 was 190 $cm^{-3}s^{-1}$, in contrast to this estimation. There was another possibility that ozone reacted with possible organic impurities in FT-2 to produce OH, which oxidized SO_2 to produce H_2SO_4 and nucleated in FT-2, but no organics were added in our experiments. It is not clear at present what is the cause of nucleation in FT-2 and this requires future study. However, it was clear that the co-presence of

ozone and SO_2 was an important factor in preventing evaporation of newly formed particles and facilitated them to the further grow at the higher temperature. The overall *GR* of particles in FT-2 was from 14.9 to 23.1 nm h^{-1}, depending on the ozone concentration. These results imply some heterogeneous reactions occurring on acidic sulfuric acid clusters, in a similar way to form sulphate from oxidation reactions of SO_2 on acidic particles as proposed by (Hung & Hoffmann, 2015).

Our results thus show that particles were observed at the end of the room temperature nucleation tube after they were initially nucleated at lower temperatures growth tube. These results can explain the presence of newly formed particles observed in Amazon forests by (Wang et al., 2016), which concluded that the particle loads observed in the boundary layer could be the result of downward transport of particles formed in the colder free troposphere. The results of our experiments thus confirm that particles can indeed nucleate at higher altitudes under colder temperatures and while transported downward to warmer surface sites, they can survive and grow further.

4. Conclusions and Implications

We have conducted experiments to study the temperature dependence of aerosol nucleation and growth using the TANGENT setup. This setup consists of two flow tubes which enable us to study nucleation and subsequent growth independently. In the nucleation tube, temperature was varied from 258 to 297 K and RH from 4% to 85%. [H_2SO_4] spanned 10^6 to 10^8 cm^{-3}, which corresponds to RA of 10^{-5} to 10^{-2}. Based on the measured [NH_3] to [H_2SO_4] ratios, it was most likely that nucleation took place via the ternary process. The growth tube was kept at room temperature and the dry condition (RH of 10%). SO_2 was present at 100 ppbv to 5 ppmv and ozone at 0 to 248 ppbv.

Our results indicate that lower temperatures enhance both nucleation and growth rates as predicted by CNT. However, the temperature effects on nucleation rates become less important at lower temperatures (below 268 K), consistent with CLOUD studies (Duplissy et al. 2016) which found that sulfuric acid nucleation takes place at the kinetic limit without a Gibbs free energy barrier when temperature was low. These results emphasize the importance of NH_3 and other ternary species at warmer temperatures, for example, especially in the conditions present in the boundary layer.

Our results demonstrate that clusters formed at lower temperatures, while being transported to warmer temperatures, can survive evaporation and even grow further in the presence of SO_2 and ozone. Thus, it is reasonable to conclude that the new particles formed in the free troposphere over the Amazon forest are transferred downward to the warmer surface to act as a reservoir of nuclei mode particles (Wang et al., 2016), though the mechanism of growth is different from the one studied here (SO_2 + ozone).

Our results also show that the further growth is strongly dependent on the ozone level, implying that some unknown heterogeneous reaction processes involving SO_2 and ozone on sulfuric clusters may play important roles in NPF. These results can open a new research avenue for future studies for better understanding the roles of heterogeneous reactions involving nanoparticles and the effects of SO_2 on the nanoparticle growth. At present, it is not known why NPF takes place with high frequency and strong magnitude in extremely polluted megacities in China under the conditions with exceedingly high loadings

of pre-existing aerosol particles (Guo et al., 2014; Yao et al., 2018; Yu et al., 2017b). The heterogeneous reactions involving SO_2 on nanoparticles proposed here may provide some key insights into understanding the frequent nucleation and fast growth observed in these regions, where there are also very high concentrations of SO_2 and ozone.

Data Availability

All data of this work can be obtained from L. Tiszenkel (lt0021@uah.edu)

Author Contributions

SL and MJ designed the experiments and LT, CS, JK, QO and MA carried them out. LT, QO and HY developed code used in the data analysis. LT, CS and QO performed the data analysis. LT and SL prepared the manuscript with contributions from all co-authors.

Acknowledgements

This work was supported by NSF Awards AGS-1649719 and AGS-1649694.

References

Almeida, J., Schobesberger, S., Kurten, A., Ortega, I. K., Kupiainen-Maatta, O., Praplan, A. P., Adamov, A., Amorim, A., Bianchi, F., Breitenlechner, M., David, A., Dommen, J., Donahue, N. M., Downard, A., Dunne, E., Duplissy, J., Ehrhart, S., Flagan, R. C., Franchin, A., Guida, R., Hakala, J., Hansel, A., Heinritzi, M., Henschel, H., Jokinen, T., Junninen, H., Kajos, M., Kangasluoma, J., Keskinen, H., Kupc, A., Kurten, T., Kvashin, A. N., Laaksonen, A., Lehtipalo, K., Leiminger, M., Leppa, J., Loukonen, V., Makhmutov, V., Mathot, S., McGrath, M. J., Nieminen, T., Olenius, T., Onnela, A., Petaja, T., Riccobono, F., Riipinen, I., Rissanen, M., Rondo, L., Ruuskanen, T., Santos, F. D., Sarnela, N., Schallhart, S., Schnitzhofer, R., Seinfeld, J. H., Simon, M., Sipila, M., Stozhkov, Y., Stratmann, F., Tome, A., Trostl, J., Tsagkogeorgas, G., Vaattovaara, P., Viisanen, Y., Virtanen, A., Vrtala, A., Wagner, P. E., Weingartner, E., Wex, H., Williamson, C., Wimmer, D., Ye, P., Yli-Juuti, T., Carslaw, K. S., Kulmala, M., Curtius, J., Baltensperger, U., Worsnop, D. R., Vehkamaki, H., and Kirkby, J.: Molecular understanding of sulphuric acid-amine particle nucleation in the atmosphere, Nature, 502, 359-363, 10.1038/nature12663 http://www.nature.com/nature/journal/v502/n7471/abs/nature12663.html#supplementary-information, 2013.

Benson, D. R., Young, L. H., Kameel, R., and Lee, S. H.: Laboratory-measured sulfuric acid and water homogeneous nucleation rates from the SO_2 + OH reaction, Geophys. Res. Lett., 35, Doi:10.1029/2008GL033387, 10.1029/2008GL033387, 2008.

Benson, D. R., Erupe, M. E., and Lee, S. H.: Laboratory-measured H_2SO_4-H_2O-NH_3 ternary homogeneous nucleation rates: initial observations Geophys. Res. Lett, 36, Doi:10.1029/2009GL038728, 10.1029/2009GL038728, 2009.

Benson, D. R., Al-Refai, M., and Lee, S.-H.: Chemical Ionization Mass Spectrometer (CIMS) for ambient measurments of Ammonia, Atmos. Meas. Tech., 3, 1133-1162, 2010.

Benson, D. R., Yu, J. H., Markovich, A., and Lee, S. H.: Ternary homogeneous nucleation of H2SO4, NH3, and H2O under conditions relevant to the lower troposphere, Atmos. Chem. Phys., 11, 4755-4766, 10.5194/acp-11-4755-2011, 2011.

Berndt, T., Sipilä, M., Stratmann, F., Petäjä, T., Vanhanen, J., Mikkilä, J., Patokoski, J., Taipale, R., Mauldin III, R. L., and Kulmala, M.: Enhancement of atmospheric H_2SO_4 / H_2O nucleation: organic oxidation products versus amines, Atmos. Chem. Phys., 14, 751-764, 10.5194/acp-14-751-2014, 2014.

Brus, D., Hyvarinen, A. P., Viisanen, Y., Kulmala, M., and Lihavainen, H.: Homogenous nucleation of sulfuric acid and water mixture: experimental setup and first results, Atmos. Chem. Phys., 10, 2631-2641, 2010.

Chen, M., Titcombe, M., Jiang, J. K., Jen, C., Kuang, C. A., Fischer, M. L., Eisele, F. L., Siepmann, J. I., Hanson, D. R., Zhao, J., and McMurry, P. H.: Acid-base chemical reaction model for nucleation rates in the polluted atmospheric boundary layer, Proc. Natl. Acad. Sci. U. S. A., 109, 18713-18718, 10.1073/pnas.1210285109, 2012.

Dunne, E. M., Gordon, H., Kürten, A., Almeida, J., Duplissy, J., Williamson, C., Ortega, I. K., Pringle, K. J., Adamov, A., Baltensperger, U., Barmet, P., Benduhn, F., Bianchi, F., Breitenlechner, M., Clarke, A., Curtius, J., Dommen, J., Donahue, N. M., Ehrhart, S., Flagan, R. C., Franchin, A., Guida, R., Hakala, J., Hansel, A., Heinritzi, M., Jokinen, T., Kangasluoma, J., Kirkby, J., Kulmala, M., Kupc, A., Lawler, M. J., Lehtipalo, K., Makhmutov, V., Mann, G., Mathot, S., Merikanto, J., Miettinen, P., Nenes, A., Onnela, A., Rap, A., Reddington, C. L. S., Riccobono, F., Richards, N. A. D., Rissanen, M. P., Rondo, L., Sarnela, N., Schobesberger, S., Sengupta, K., Simon, M., Sipilä, M., Smith, J. N., Stozkhov, Y., Tomé, A., Tröstl, J., Wagner, P. E., Wimmer, D., Winkler, P. M., Worsnop, D. R., and Carslaw, K. S.: Global atmospheric particle formation from CERN CLOUD measurements, Science, 354, 1119-1123, 2016.

Duplissy, J., Merikanto, J., Franchin, A., Tsagkogeorgas, G., Kangasluoma, J., Wimmer, D., Vuollekoski, H., Schobesberger, S., Lehtipalo, K., Flagan, R. C., Brus, D., Donahue, N. M., Vehkamäki, H., Almeida, J., Amorim, A., Barmet, P., Bianchi, F., Breitenlechner, M., Dunne, E. M., Guida, R., Henschel, H., Junninen, H., Kirkby, J., Kürten, A., Kupc, A., Määttänen, A., Makhmutov, V., Mathot, S., Nieminen, T., Onnela, A., Praplan, A. P., Riccobono, F., Rondo, L., Steiner, G., Tome, A., Walther, H., Baltensperger, U., Carslaw, K. S., Dommen, J., Hansel, A., Petäjä, T., Sipilä, M., Stratmann, F., Vrtala, A., Wagner, P. E., Worsnop, D. R., Curtius, J., and Kulmala, M.: Effect of ions on sulfuric acid-water binary particle formation: 2. Experimental data and comparison with QC-normalized classical nucleation theory, J. Geophys. Res., 121, 1752-1775, 10.1002/2015JD023539, 2016.

Erupe, M. E., Viggiano, A. A., and Lee, S. H.: The effect of trimethylamine on atmospheric nucleation involving H_2SO_4, Atmos. Chem. Phys., 11, 4767-4775, 2011.

Glasoe, W. A., Volz, K., Panta, B., Freshour, N., Bachman, R., Hanson, D. R., McMurry, P. H., and Jen, C.: Sulfuric acid nucleation: an experimental study of the effect of seven bases, J. Geophys. Res., 120, 1933-1950, 10.1002/2014JD022730, 2015.

Gordon, H., Kirkby, J., Baltensperger, U., Bianchi, F., Breitenlechner, M., Curtius, J., Dias, A., Dommen, J., Donahue, N. M., Dunne, E. M., Duplissy, J., Ehrhart, S., Flagan, R. C., Frege, C., Fuchs, C., Hansel, A., Hoyle, C. R., Kulmala, M., Kurten, A., Lehtipalo, K., Makhmutov, V., Molteni, U., Rissanen, M. P., Stozkhov, Y., Trostl, J., Tsagkogeorgas, G., Wagner, R., Williamson, C., Wimmer, D., Winkler, P. M., Yan, C., and Carslaw, K. S.: Causes and importance of new particle formation in the present-day and preindustrial atmospheres, J. Geophys. Res., 122, 8739-8760, 10.1002/2017jd026844, 2017.

Guo, S., Hu, M., Zamora, M. L., Peng, J., Shang, D., Zheng, J., Du, Z., Wu, Z., Shao, M., Zeng, L., Molina, M. J., and Zhang, R.: Elucidating severe urban haze formation in China, Proceedings of the National Academy of Sciences, 111, 17373-17378, 2014.

Hanson, D. R., Bier, I., Panta, B., Jen, C. N., and McMurry, P. H.: Computational Fluid Dynamics Studies of a Flow Reactor: Free Energies of Clusters of Sulfuric Acid with NH3 or Dimethyl Amine, J. Phys. Chem. A, 121, 3976-3990, 10.1021/acs.jpca.7b00252, 2017.

Hung, H.-M., and Hoffmann, M. R.: Oxidation of gas-phase SO2 on the surfaces of acidic microdroplets: Implications for sulfate and sulfate radical anion formation in the atmospheric liquid phase, Environ. Sci. Technol., 49, 13768-13776, 2015.

Jen, C. N., McMurry, P. H., and Hanson, D. R.: Stabilization of sulfuric acid dimers by ammonia, methylamine, dimethylamine, and trimethylamine, J. Geophys. Res., 119, Doi: 10.1002/2014jd021592, 10.1002/2014jd021592, 2014.

Jen, C. N., Zhao, J., McMurry, P. H., and Hanson, D. R.: Chemical ionization of clusters formed from sulfuric acid and dimethylamine or diamines, Atmos. Chem. Phys., 16, 12513-12529, 10.5194/acp-16-12513-2016, 2016.

Kanawade, V. P., Jobson, B. T., Guenther, A. B., Erupe, M. E., Pressley, S. N., Tripathi, S. N., and Lee, S. H.: Isoprene suppression of new particle formation in a mixed deciduous forest, Atmos. Chem. Phys., 11, 6013-6027, 10.5194/acp-11-6013-2011, 2011.

Kashchiev, D.: On the relation between nucleation work, nucleus size, and nucleation rate, J. Phys. Chem., 76, 5098-5012, 1982.

Kirkby, J., Curtius, J., Almeida, J., Dunne, E., Duplissy, J., Ehrhart, S., Franchin, A., Gagne, S., Ickes, L., Kurten, A., Kupc, A., Metzger, A., Riccobono, F., Rondo, L., Schobesberger, S., Tsagkogeorgas, G., Wimmer, D., Amorim, A., Bianchi, F., Breitenlechner, M., David, A., Dommen, J., Downard, A., Ehn, M., Flagan, R. C., Haider, S., Hansel, A., Hauser, D., Jud, W., Junninen, H., Kreissl, F., Kvashin, A. N., Laaksonen, A., Lehtipalo, K., Lima, J., Lovejoy, E. R., Makhmutov, V., Mathot, S., Mikkila, J., Minginette, P., Mogo, S., Nieminen, T., Onnela, A., Pereira, P., Petaja, T., Schnitzhofer, R., Seinfeld, J. H., Sipila, M., Stozhkov, Y., Stratmann, F., Tome, A., Vanhanen, J., Viisanen, Y., Vrtala, A., Wagner, P. E., Walther, H., Weingartner, E., Wex, H., Winkler, P. M., Carslaw, K. S., Worsnop, D. R., Baltensperger, U., and Kulmala, M.: Role of sulphuric acid,

ammonia and galactic cosmic rays in atmospheric aerosol nucleation, Nature, 476, 429-433, http://www.nature.com/nature/journal/v476/n7361/abs/nature10343.html#supplementary-information, 2011.

Krasnomowitz, J. M., Apsokardu, M. J., Stangl, C. M., Tiszenkel, L, Ouyang, Q, Lee, S. H., and Johnston, V. M.: Growth of ammonium sulfate seed particles in the Aitken mode size range by α-pinene ozonolysis, Aerosol Science and Technology, 2018. Under review.

Kulmala, M., Kontkanen, J., Junninen, H., Lehtipalo, K., Manninen, H. E., Nieminen, T., Petäjä, T., Sipilä, M., Schobesberger, S., Rantala, P., Franchin, A., Jokinen, T., Järvinen, E., Äijälä, M., Kangasluoma, J., Hakala, J., Aalto, P. P., Paasonen, P., Mikkilä, J., Vanhanen, J., Aalto, J., Hakola, H., Makkonen, U., Ruuskanen, T., Mauldin, R. L., Duplissy, J., Vehkamäki, H., Bäck, J., Kortelainen, A., Riipinen, I., Kurtén, T., Johnston, M. V., Smith, J. N., Ehn, M., Mentel, T. F., Lehtinen, K. E. J., Laaksonen, A., Kerminen, V. M., and Worsnop, D. R.: Direct observations of atmospheric aerosol nucleation, Science, 339, 943-946, 10.1126/science.1227385, 2013.

Kulmala, M., Kerminen, V.-M., Petaja, T., Ding, A., and Wang, L.: Atmospheric gas-to-particle conversion: why NPF events are observed in megacities?, Faraday Discussions, Doi: 10.1039/C1036FD00257A, 10.1039/c6fd00257a, 2017.

Kürten, A., Bianchi, F., Almeida, J., Kupiainen-Määttä, O., Dunne, E. M., Duplissy, J., Williamson, C., Barmet, P., Breitenlechner, M., Dommen, J., Donahue, N. M., Flagan, R. C., Franchin, A., Gordon, H., Hakala, J., Hansel, A., Heinritzi, M., Ickes, L., Jokinen, T., Kangasluoma, J., Kim, J., Kirkby, J., Kupc, A., Lehtipalo, K., Leiminger, M., Makhmutov, V., Onnela, A., Ortega, I. K., Petäjä, T., Praplan, A. P., Riccobono, F., Rissanen, M. P., Rondo, L., Schnitzhofer, R., Schobesberger, S., Smith, J. N., Steiner, G., Stozhkov, Y., Tomé, A., Tröstl, J., Tsagkogeorgas, G., Wagner, P. E., Wimmer, D., Ye, P., Baltensperger, U., Carslaw, K., Kulmala, M., and Curtius, J.: Experimental particle formation rates spanning tropospheric sulfuric acid and ammonia abundances, ion production rates, and temperatures, J. Geophys. Res., 121, 12,377-312,400, 10.1002/2015JD023908, 2016.

Lee, S.-H., Uin, J., Guenther, A. B., Gouw, J. A. d., Yu, F., Nadykto, A. B., Herb, J., Ng, N. L., Koss, A., Brune, W. H., Baumann, K., Kanawad, V. P., Keutsch, F. N., Nenes, A., Olsen, K., Goldstein, A., and Qi, O.: Isoprene suppression of new particle formation: Potential mechanism and implications, J. Geophys. Res., 121, Doi:10.1029/2016JD024844 10.1029/2016JD024844 2016.

Martin, S. T., Artaxo, P., Machado, L., Manzi, A. O., Souza, R. A. F., Schumacher, C., Wang, J., Biscaro, T., Brito, J., Calheiros, A., Jardine, K., Medeiros, A., Portela, B., de Sá, S. S., Adachi, K., Aiken, A. C., Albrecht, R., Alexander, L., Andreae, M. O., Barbosa, H. M. J., Buseck, P., Chand, D., Comstock, J. M., Day, D. A., Dubey, M., Fan, J., Fast, J., Fisch, G., Fortner, E., Giangrande, S., Gilles, M., Goldstein, A. H., Guenther, A., Hubbe, J., Jensen, M., Jimenez, J. L., Keutsch, F. N., Kim, S., Kuang, C., Laskin, A., McKinney, K., Mei, F., Miller, M., Nascimento, R., Pauliquevis, T., Pekour, M., Peres, J., Petäjä, T., Pöhlker, C., Pöschl, U., Rizzo, L., Schmid, B., Shilling, J. E., Dias, M. A. S., Smith, J. N., Tomlinson, J. M., Tóta, J., and Wendisch, M.: The Green Ocean Amazon Experiment (GoAmazon2014/5) Observes Pollution Affecting Gases, Aerosols, Clouds, and Rainfall over the Rain Forest, Bulletin of the American Meteorological Society, 98, 981-997, 10.1175/BAMS-D-15-00221.1, 2016.

McGraw, R., and Zhang, R.: Multivariate analysis of homogeneous nucleation rate measurements. Nucleation in the p-toluic acid/sulfuric acid/water system, J. Chem. Phys., 128, Doi: 10.1063/1061.2830030, 10.1063/1.2830030, 2008.

Merikanto, J., Spracklen, D. V., Mann, G. W., Pickering, S. J., and Carslaw, K. S.: Impact of nucleation on global CCN, Atmos. Chem. Phys., 9, 8601-8616, 2009.

Rizzo, V. L., Roldin, P., Brito, J., Backman, J., Swietlicki, E., Krejci, R., Tunved, P., Petäjä, T., Kulmala, M., and Artaxo, P.: Multi-year statistical and modeling analysis of submicrometer aerosol number size distributions at a rain forest site in Amazonia, Atmos. Chem. Phys., 18, 10255-10274, 10.5194/acp-18-10255-2018, 2018.

Schobesberger, S., Franchin, A., Bianchi, F., Rondo, L., Duplissy, J., Kürten, A., Ortega, I. K., Metzger, A., Schnitzhofer, R., Almeida, J., Amorim, A., Dommen, J., Dunne, E. M., Ehn, M., Gagné, S., Ickes, L., Junninen, H., Hansel, A., Kerminen, V. M., Kirkby, J., Kupc, A., Laaksonen, A., Lehtipalo, K., Mathot, S., Onnela, A., Petäjä, T., Riccobono, F., Santos, F. D., Sipilä, M., Tomé, A., Tsagkogeorgas, G., Viisanen, Y., Wagner, P. E., Wimmer, D., Curtius, J., Donahue, N. M., Baltensperger, U., Kulmala, M., and Worsnop, D. R.: On the composition of ammonia–sulfuric-acid ion clusters during aerosol particle formation, Atmos. Chem. Phys., 15, 55-78, 10.5194/acp-15-55-2015, 2015.

Seinfeld, J. H., and Pandis, S. N.: Atmospheric chemistry and physics: from air pollution to climate change, John Wiley and Sons, Inc., New Jersey, 2016.

Skrabalova, L., Brus, D., Anttila, T., Zdimal, V., and Lihavainen, H.: Growth of sulphuric acid nanoparticles under wet and dry conditions, Atmos. Chem. Phys., 14, 6461-6475, 10.5194/acp-14-6461-2014, 2014.

Wang, M., and Penner, J. E.: Aerosol indirect forcing in a global model with particle nucleation, Atmos. Chem. Phys., 9, 239-260, 2009.

Wang, J., Krejci, R., Giangrande, S., Kuang, C., Barbosa, H. M. J., Brito, J., Carbone, S., Chi, X., Comstock, J., Ditas, F., Lavric, J., Manninen, H. E., Mei, F., Moran-Zuloaga, D., Pöhlker, C., Pöhlker, M. L., Saturno, J., Schmid, B., Souza, R. A. F., Springston, S. R., Tomlinson, J. M., Toto, T., Walter, D., Wimmer, D., Smith, J. N., Kulmala, M., Machado, L. A. T., Artaxo, P., Andreae, M. O., Petäjä, T., and Martin, S. T.: Amazon boundary layer aerosol concentration sustained by vertical transport during rainfall, Nature, 539, 416-419, 10.1038/nature19819, 2016.

Yao, L., Garmash, O., Bianchi, F., Zheng, J., Yan, C., Kontkanen, J., Junninen, H., Mazon, S. B., Ehn, M., Paasonen, P., Sipila, M., Wang, M. Y., Wang, X. K., Xiao, S., Chen, H. F., Lu, Y. Q., Zhang, B. W., Wang, D. F., Fu, Q. Y., Geng, F. H., Li, L., Wang, H. L., Qiao, L. P., Yang, X., Chen, J. M., Kerminen, V. M., Petaja, T., Worsnop, D. R., Kulmala, M., and Wang, L.: Atmospheric new particle formation from sulfuric acid and amines in a Chinese megacity, Science, 361, 278-281, 10.1126/science.aao4839, 2018.

You, Y., Kanawade, V. P., de Gouw, J. A., Guenther, A. B., Madronich, S., Sierra-Hernández, M. R., Lawler, M., Smith, J. N., Takahama, S., Ruggeri, G., Koss, A., Olson, K., Baumann, K., Weber, R. J., Nenes, A., Guo, H., Edgerton, E. S., Porcelli, L., Brune, W. H., Goldstein, A. H., and Lee, S. H.: Atmospheric amines and ammonia measured with a Chemical Ionization Mass Spectrometer (CIMS), Atmos. Chem. Phys. , 14, 12181-12194, 10.5194/acpd-14-16411-2014, 2014.

Young, L. H., Benson, D. R., Rifkha, F., Pierce, J. R., Junninen, H., Kulmala, M., and Lee, S. H.: Laboratory studies of sulfuric acid and water binary homogeneous nucleation: evaluation of laboratory setup and preliminary results, Atmos. Chem. Phys., 8, 1-20, 2008.

Yu, F., and Luo, G.: Simulation of particle size distribution with a global aerosol model: contribution of nucleation to aerosol and CCN number concentrations, Atmos. Chem. Phys., 9, 7691-7710, 10.5194/acp-9-7691-2009, 2009.

Yu, H., and Lee, S.-H.: Chemical ionisation mass spectrometry for the measurement of atmospheric amines, Environmental Chemistry, 9, 190-201, 2012.

Yu, H., McGraw, R., and Lee, S. H.: Effects of amines on formation of sub-3 nm particles and their subsequent growth, Geophys. Res. Lett., 39, Doi: 10.1029/2011gl050099, 10.1029/2011gl050099, 2012.

Yu, F., Luo, G., Pryor, S. C., Pillai, P. R., Lee, S. H., Ortega, J., Schwab, J. J., Hallar, A. G., Leaitch, W. R., Aneja, V. P., Smith, J. N., Walker, J. T., Hogrefe, O., and Demerjian, K. L.: Spring and summer contrast in new particle formation over nine forest areas in North America, Atmos. Chem. Phys., 15, 13993-14003, 10.5194/acpd-15-21271-2015, 2015.

Yu, H., Dai, L., Zhao, Y., Kanawade, V. P., Tripathi, S. N., Ge, X., Chen, M., and Lee, S.-H.: Laboratory observations of temperature and humidity dependencies of nucleation and growth rates of sub-3 nm particles, J. Geophys. Res., 122, 1919-1929, 10.1002/2016JD025619, 2017.

Yu, H., Ren, L., and Kanawade, V. P.: New Particle Formation and Growth Mechanisms in Highly Polluted Environments, Current Pollution Reports, 3, 245-253, 10.1007/s40726-017-0067-3, 2017.

Zhang, R., Khalizov, A. F., Wang, L., Hu, M., and Xu, W.: Nucleation and growth of nanoparticles in the atmosphere, Chem. Rev., 112, 957-2011, 2012.

Zollner, J. H., Glasoe, W. A., Panta, B., Carlson, K. K., McMurry, P. H., and Hanson, D. R.: Sulfuric acid nucleation: power dependencies, variation with relative humidity, and effect of bases, Atmos. Chem. Phys., 12, 4399-4411, 10.5194/acpd-12-1117-2012, 2012.

Atmos. Chem. Phys. Discuss., https://doi.org/10.5194/acp-2019-3
Manuscript under review for journal Atmos. Chem. Phys.
Discussion started: 7 January 2019

Atmospheric Chemistry and Physics Discussions

Table 1. Typical experimental conditions used in FT-1 and FT-2. *J* in FT-1 is the nucleation rate for sub-2 nm particles. *J* in FT-2 is the formation rate of total particles in the size range from 3 to 60 nm; the particle mean diameter ranged from 2.7 to 3.4 nm depending on the ozone concentration. *GR* in FT-1 is the growth rate of sub-3 nm particles. *GR* in FT-2 is the growth rate of total particles from 3 to 60 nm. NH_3 and amine measurements are from IOP 2017 under similar conditions.

FT-1: Nucleation Region						FT-2: Growth Region	
Temperature (K)	297	288	278	268	258	Temperature (K)	297
RH	20% - 45%	8% - 60%	12% - 80%	23% - 80%	46% - 85%	RH	10%
$[H_2SO_4]$ (cm^{-3})	1×10^7 – 3×10^8	7×10^6 – 2×10^8	2×10^6 – 7×10^7	2×10^6 – 4×10^7	4×10^6 – 7×10^7	SO_2 (ppbv)	100-5000
RA	4×10^{-5} – 7×10^{-4}	7×10^{-5} – 1×10^{-3}	6×10^{-5} – 2×10^{-3}	3×10^{-4} – 5×10^{-3}	3×10^{-3} – 4×10^{-2}	O_3 (ppbv)	0 - 248
GR (nm h^{-1})	1 - 20	1 - 20	2 - 80	3 - 45	2 – 35	GR (nm h^{-1})	14.9 - 23.1
J (cm^{-3} s^{-1})	10^1 – 10^5	10^2 – 10^5	10^2 – 10^5	10^2 – 10^5	10^2 – 10^5	J (cm^{-3} s^{-1})	189.9
$[NH_3]$ (pptv)	14.2 ± 6.9						
$[NH_3]/[H_2SO_4]$	0.6 – 52.7	0.9 – 75.2	2.6 - 263	4.5 - 263	2.6 – 132		
[C1 amine] (pptv)	4.5 ± 2.60						
[C2 amine] (pptv)	44.8 ± 41.8						
[C3 amine] (pptv)	7.27 ± 2.50						
[C4 amine] (pptv)	21.7 ± 7.5						
[C5 amine] (pptv)	13.9 ± 4.3						
[C6 amine] (pptv)	8.42 ± 1.8						

Atmos. Chem. Phys. Discuss., https://doi.org/10.5194/acp-2019-3
Manuscript under review for journal Atmos. Chem. Phys.
Discussion started: 7 January 2019

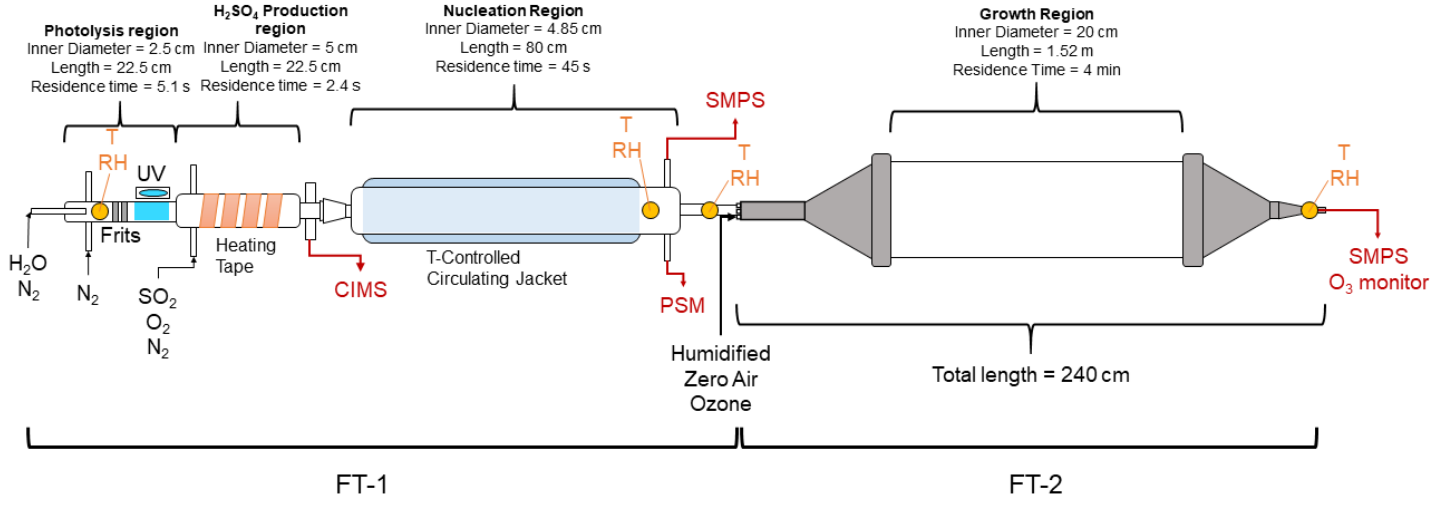

Figure 1. Schematic diagram of the TANGENT experimental setup. This setup consists of two flow tubes (FT). T indicates temperature. FT-1 is used as the nucleation region and FT-2 as the growth region. Table 1 shows the typical experimental conditions used during the 2018 IOP study.

Atmos. Chem. Phys. Discuss., https://doi.org/10.5194/acp-2019-3
Manuscript under review for journal Atmos. Chem. Phys.
Discussion started: 7 January 2019

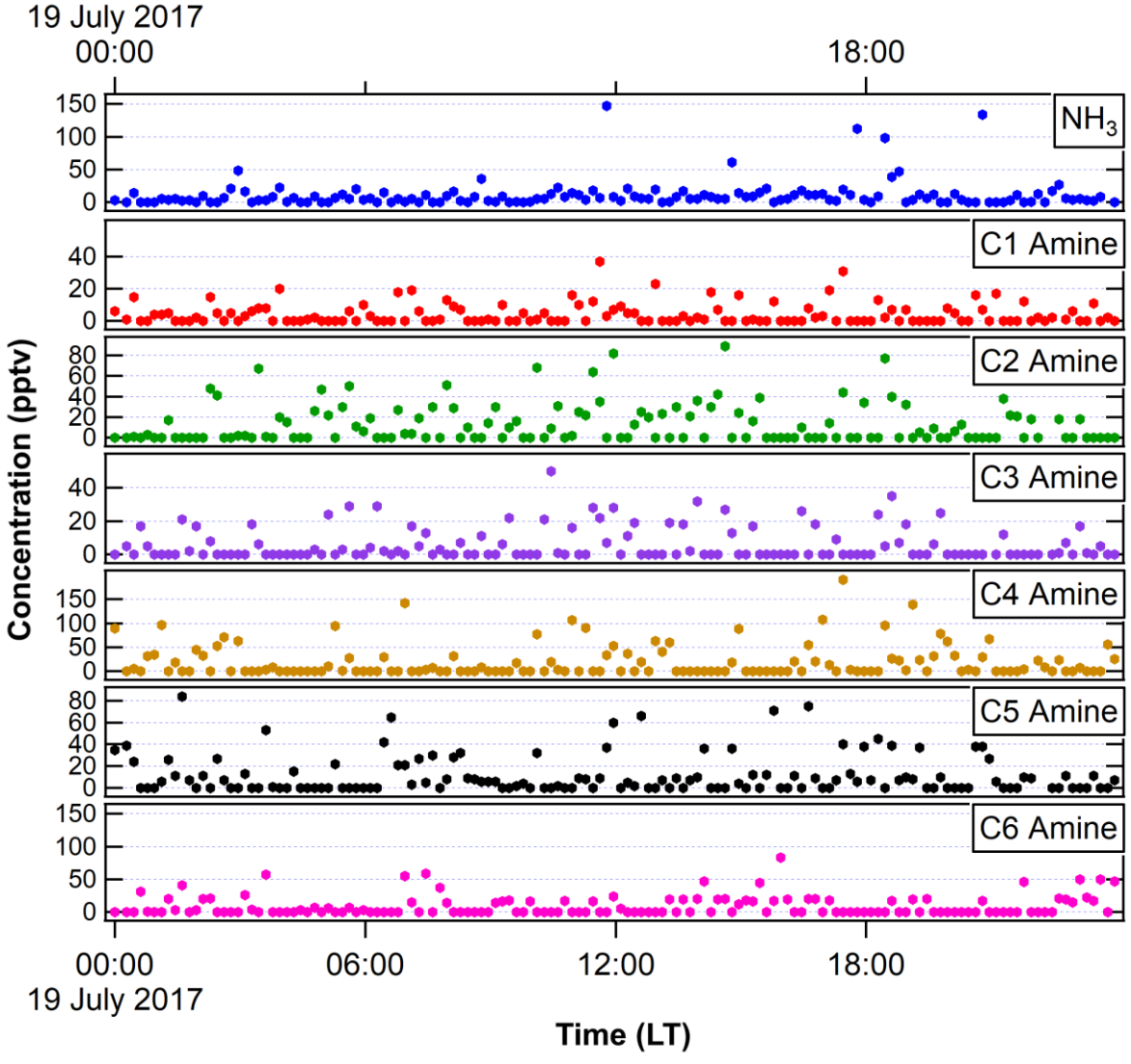

Figure 2. NH_3 and amines measured with the ethanol-CIMS in the FT-1 during the 2017 IOP in a very similar experimental condition as in 2018 IOP. We show here an example of one day measurements (July 19, 2017).

Atmos. Chem. Phys. Discuss., https://doi.org/10.5194/acp-2019-3
Manuscript under review for journal Atmos. Chem. Phys.
Discussion started: 7 January 2019

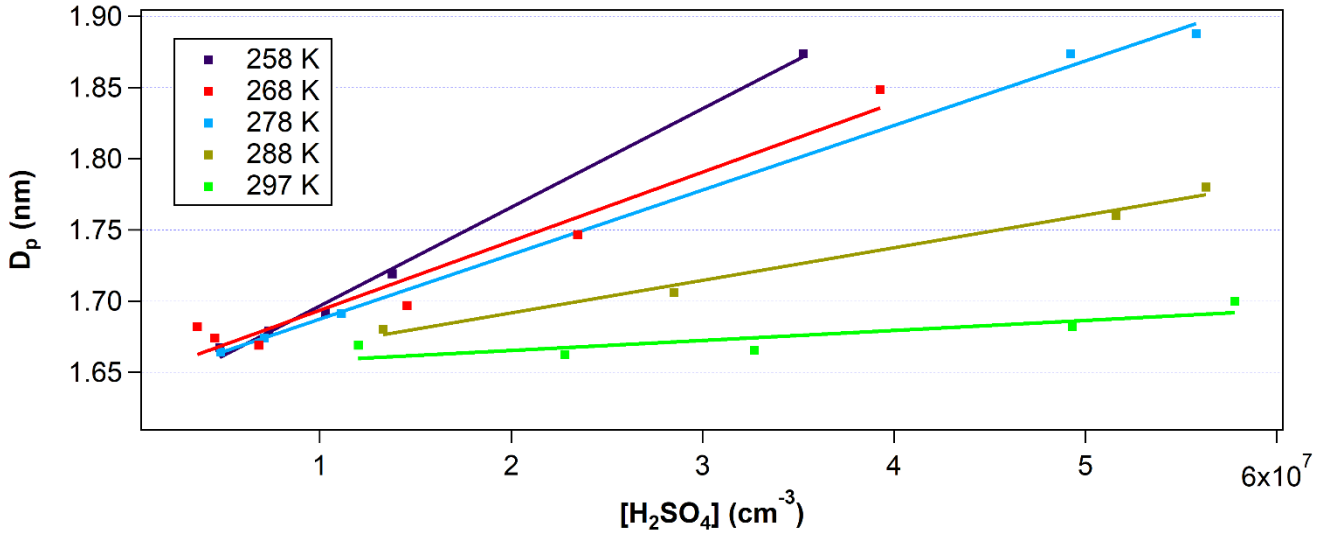

Figure 3. Mean diameter of particles (D_p) inverted from the PSM measurements at the end of the nucleation tube as a function of [H_2SO_4] and temperature. Data points were taken at RH between 20% and 30%. Solid lines are linear fittings of the measurement data (coloured squares) under different temperatures.

Atmos. Chem. Phys. Discuss., https://doi.org/10.5194/acp-2019-3
Manuscript under review for journal Atmos. Chem. Phys.
Discussion started: 7 January 2019

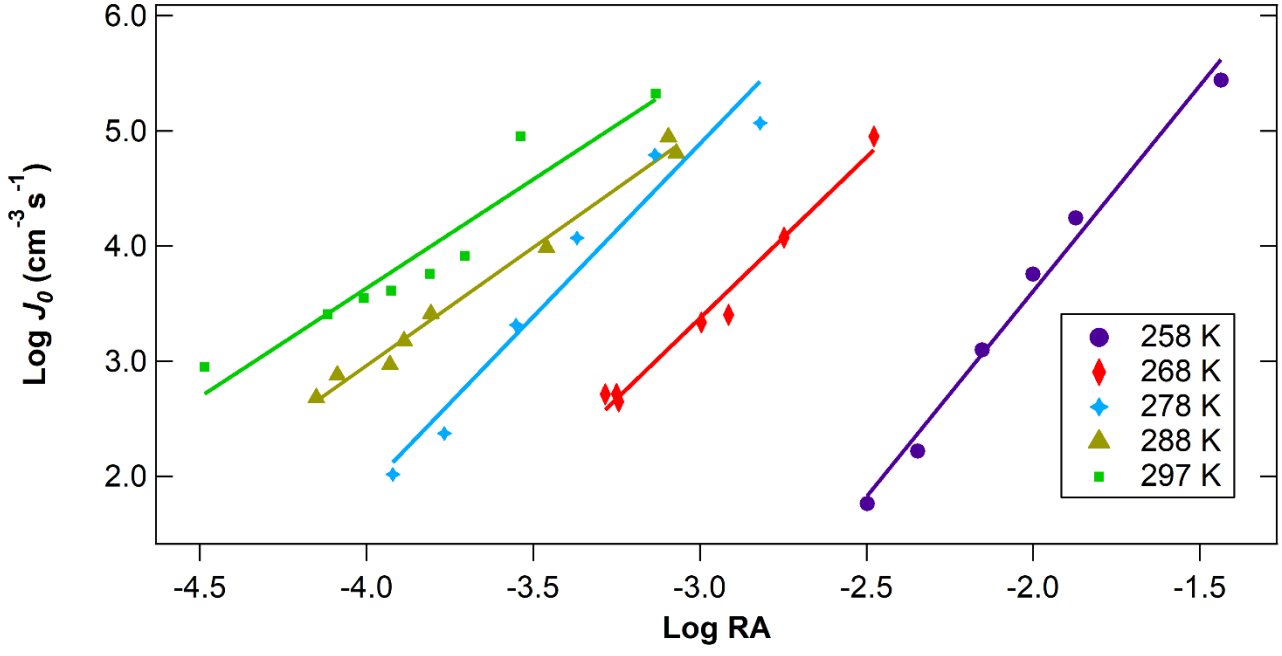

Figure 4. Log J_0 vs. Log RA for different temperatures at a relatively constant RH (41% - 45%). Temperatures ranged from 258 to 297 K.

Atmos. Chem. Phys. Discuss., https://doi.org/10.5194/acp-2019-3
Manuscript under review for journal Atmos. Chem. Phys.
Discussion started: 7 January 2019

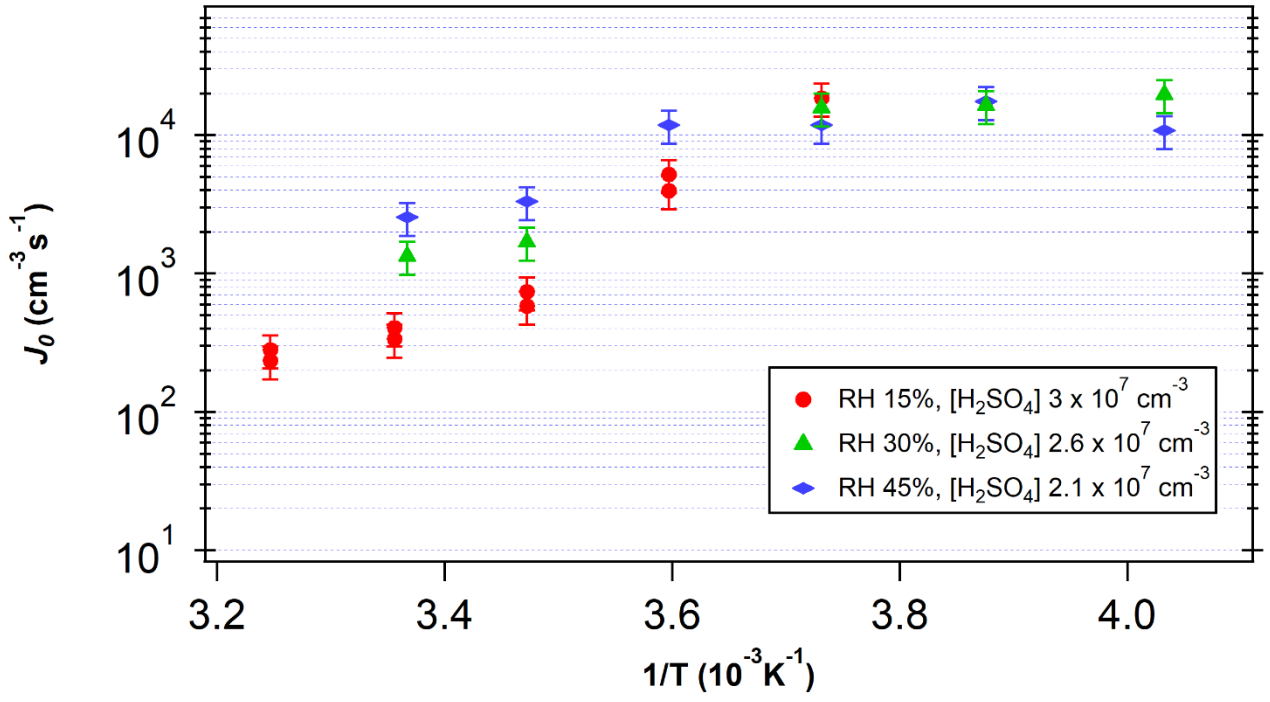

Figure 5. Log J_0 vs. 1/T for [H_2SO_4] between 2x10^7 and 3x10^7 cm^{-3}. T is the temperature in FT-1. RH ranged from 15% to 45%. Vertical bars indicate one standard deviation of the measured nucleation rates.

Atmos. Chem. Phys. Discuss., https://doi.org/10.5194/acp-2019-3
Manuscript under review for journal Atmos. Chem. Phys.
Discussion started: 7 January 2019

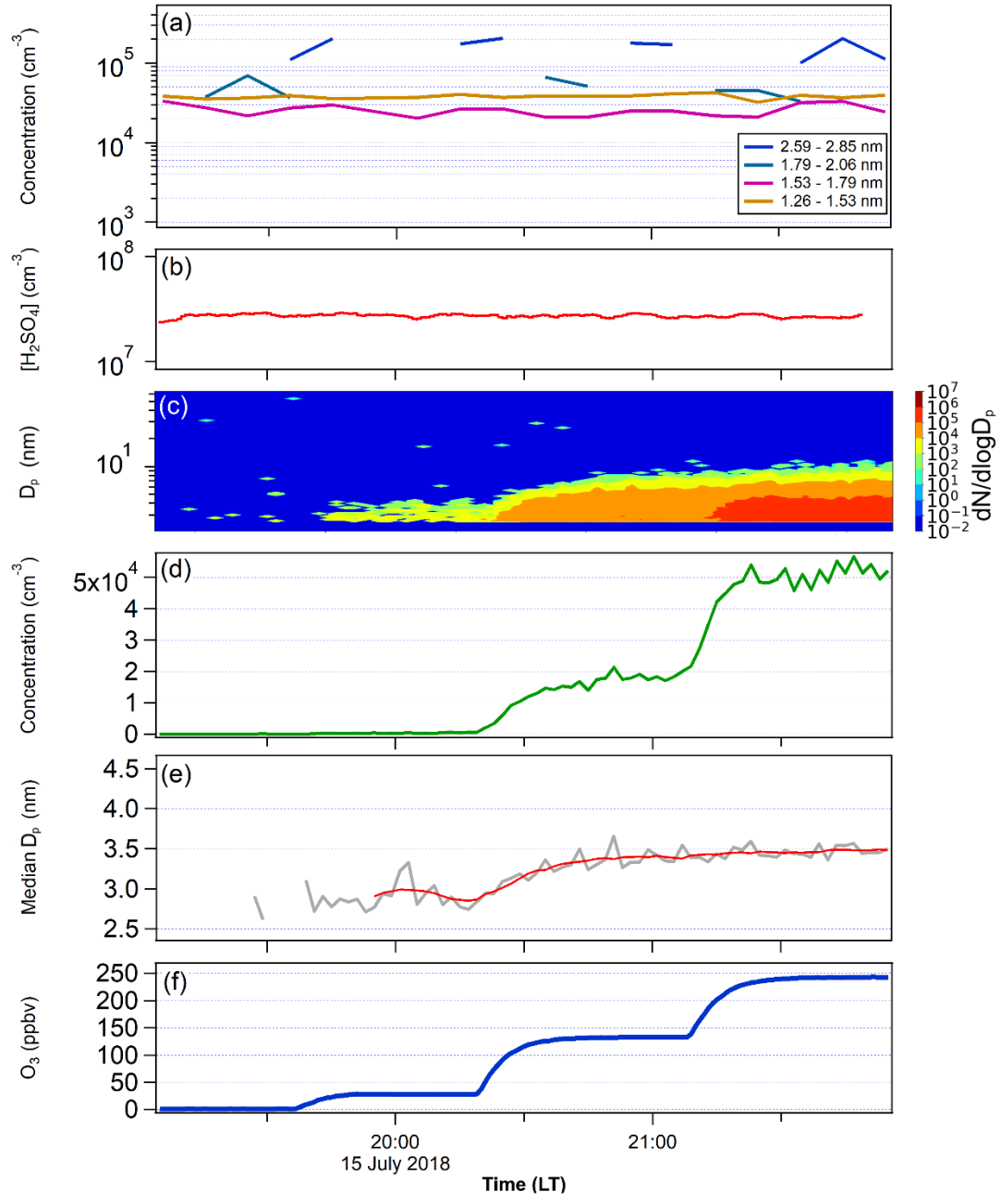

Figure 6. (a) The PSM-inverted size distribution and (b) [H_2SO_4] measured in FT-1. FT-1 was at 268 K, residence time 45 s. Total concentration at the end of FT-1 was 1.79 x 10^5 cm^{-3} with a mean D_p of 1.91 nm. (c) SMPS-measured particle size distribution, (d) total number concentration, (e) the particle median diameter D_p, and (f) O_3 concentrations in FT-2. FT-2 was kept at 297 K, and the residence time was 4 min. The red line in (e) indicates the average values of D_p. SO_2 was 500 and 83 ppbv in FT-1 and FT-2, respectively. H_2SO_4 was not measured at FT-2; however, after considering wall loss in FT-1 and the 1:6 dilution FT-2, [H_2SO_4] in FT-2 was estimated to be 1.15 x 10^6 cm^{-3}.